INSTITUTE OF PLASMA PHYSICS

NAGOYA UNIVERSITY

RESEARCH REPORT

NAGOYA, JAPAN

Trapped-Ion Instabilities in Ion-Acoustic Wave

H. Ikezi, Y. Kiwamoto

K. Nishikawa* and K. Mima**

IPPJ-120

February 1972

Further communication about this report is to be sent to the Research Information Center, Institute of Plasma Physics, Nagoya University, Nagoya, JAPAN.

Permanent Address * : Department of Physics, Hiroshima University, Hiroshima, Japan

**: Department of Physics, Kyoto University, Kyoto, Japan

Abstract

Growth of two types of sideband waves has been observed experimentally when a relatively large-amplitude ion-acoustic wave propagates in a collisionless plasma having the electron to ion temperature ratio $T_e/T_i \gtrsim 20$. The theory of the trapped-particle instability well accounts for the frequency spectrum and the frequency and the amplitude ranges of the large-amplitude wave, where the sideband waves grow, and also their growth rates. The sidebands extract the energy from the large-amplitude wave and cause its heavy damping.

1. Introduction

The stability of a nonlinear stationary electrostatic wave[1] (B-G-K wave) has been received considerable attention in recent years. Since Wharton, Malmberg and O'Neil[2] observed the growth of a sideband wave to a large-amplitude electron plasma wave, the theoretical works[3-7] pointed out that the particles trapped in the potential troughs of a large-amplitude wave induce the instability. Though many theoretical works and computer simulations[8,9] have been reported, no relevant experiments have been done except for Ref.2. Compared to the time when Ref.2 appeared, we are now at a position to perform more detailed experiments of the trapped-particle instability. In addition to the theoretical progress, the method to excite the ion-acoustic wave, developed for the collisionless shock wave studies,[10,11] makes us possible to carry out the large-amplitude wave experiments.

Physically, the trapped-particle instability can be viewed as a parametric instability between upper and lower sideband of a large-amplitude wave through the bouncing motion of the trapped-particles in the electric potential troughs of the large-amplitude wave (hereafter to be referred to as the carrier wave). The coupling is strengthened when the bouncing motion is resonant with the sideband wave (ω,k), i.e. when the sideband frequency in the reference frame moving with the carrier wave, $\Omega \equiv \omega - k\omega_0/k_0$, equals the bounce frequency $\pm\omega_B$. Here ω_0 and k_0 are the frequency and the wavenumber of the carrier wave. Let us look at the behavior of the particle distribution function in the presence

of the carrier wave. The theory of Al'tsul and Karpman[12] which is based on the collisionless Boltzman equation shows that the distribution near the phase velocity of the carrier wave has resonances at $\sqrt{2N+1}\,\omega_B$, where N is a non-negative integer.[13] Therefore, the coupling of the sideband to the carrier wave is considered to be strong when Ω is equal to $\pm\sqrt{2N+1}\,\omega_B$. If the wave amplitudes are not very large so that the dispersion relation of the wave is well described by the linear theory, the frequency of the unstable wave is determined by the above resonance condition together with the dispersion relation. Indeed Ref.7 predicts that, in the weak-coupling limit, i.e. when the trapped-particle density is sufficiently low, a couple of modes specified by (ω,k) and $(\omega - 2\omega_0,\ k - 2k_0)$, $(k < k_0)$, grow when one of the following conditions is satisfied:

$$\text{(i)}\quad \frac{\omega_0}{k_0} \simeq \frac{\omega - \sqrt{2N+1}\,\omega_B}{k} \quad \text{and} \quad \varepsilon(k,\omega) \simeq 0, \qquad \text{(1a)}$$

$$\text{(ii)}\quad \frac{\omega_0}{k_0} \simeq \frac{\omega - \sqrt{2N+1}\,\omega_B}{k} \quad \text{and} \quad \varepsilon(k-2k_0,\ \omega-2\omega_0) \simeq 0, \qquad \text{(1b)}$$

where $\varepsilon(k,\omega)$ is the dielectric function. In addition to these, another type of instability is predicted when

$$\text{(iii)}\quad \varepsilon(k,\omega) \simeq 0 \quad \text{and} \quad \varepsilon(k-2k_0,\ \omega-2\omega_0) \simeq 0. \qquad (2)$$

In the case of ion-acoustic wave, we are interested in the dynamics of the ions. Under the present experimental conditions, the e-e collision free-path of the electrons which

are resonant with the wave is typically of order of magnitude 10^{-2} cm, which is much shorter than the wavelength, so that the electron bouncing effects can be neglected. The dielectric function for the ion-acoustic wave can then be written approximately as[14]

$$\varepsilon(k,\omega) \simeq 1 + \frac{k_D^2}{k^2}\left[1 - \frac{T_e}{2T_i} Z'\left(\frac{\omega}{kv_i}\right)\right], \qquad (3)$$

with the approximation including the neglect of nonlinear effects. The standard notations are used. We are interested in the situation in which both the carrier and the sideband waves approximately satisfy the above ion-acoustic wave dispersion relation. The two mutually conjugate modes, (ω,k) and $(\omega - 2\omega_0, k - 2k_0)$, grow with the same growth rate and their amplitude ratio is given by $|\psi_\omega/\psi_{\omega-2\omega_0}| \simeq |\varepsilon(k-2k_0, \omega-2\omega_0)/\varepsilon(k,\omega)|$. Then if the mode (ω,k) is a lower sideband which satisfies (1a), its conjugate mode $(\omega-2\omega_0, k-2k_0)$ becomes a small-amplitude upper sideband. Note that the latter one should not be confused with the mode which satisfies (1b). Besides the necessary condition Eqs.(1) and (2), the growth rate of the wave is determined mainly by the details of the trapped-ion distribution.[7]

Experiment was carried out to observe growth of the sideband waves in the presence of a relatively large-amplitude ion-acoustic wave in a DP plasma.[10] The results are in reasonable agreement with the above theory. Details of the experiment and comparison with the theory developed by two of the present authors are described below.

2. Plasma and Wave Excitation

A plasma with a relatively high electron-to-ion temperature ratio, $T_e/T_i \simeq 20$, is employed for the following reasons: (a) The ions are trapped only when the linear spatial Landau damping rate k_L is smaller than $k_0\omega_B/\omega_0$. (b) The wave has to be dispersive, otherwise Eq.(1) cannot be satisfied.

The experiment was carried out in the DP-Machine represented in Fig.1. The apparatus consists of two identical but electrically independent conducting vacuum chambers, made of 50 cm diameter cylinders of length 40 cm each. A fine mesh grid (40 wires/cm) partitions the space into two regions. The filaments near to the inside walls of the chambers serve as the source of the primary electrons (30 - 60 eV) that produce a plasma by electron bomberdment of a neutral argon gas. The presence of primary electron currents has no adverse effect on the plasma production; they do not cause intolerable instabilities. The spontaneous density fluctuations amount to 10^{-5} of the average density. The plasma is uniform over the chamber. The plasma parameters are as follows: The plasma density $n \sim 10^9$ cm^{-3}; the electron temperature $T_e \simeq$ 3 eV; the ion temperature $T_i \simeq 0.1 - 0.2$ eV; the argon gas pressure, $(2\text{-}5) \times 10^{-4}$ Torr. For these values of the parameters, ion-ion and ion-neutral collisions can be neglected. The plasma diameter (50 cm) is much greater than the characteristic length of the wave, so that we can excite a plane wave.

The wave excitation scheme is as follows. The two plasma regions are separated by a negatively biased mesh grid such

that the electrons are prevented from short circuiting the plasma. The application of a potential difference between the plasmas introduces a fraction of the driver plasma into the target plasma. Figure 2 shows the DC characteristic of the system which reveals how the driver plasma potential V_{ex}, respect to the target plasma potential, changes the target plasma parameters. Both the ion energy analyzer[15] [Fig.2(b)] and the Langmuir probe [Fig.2(a)] curves show that the plasma potential and the density are increased when V_{ex} is positive (and vice versa) without forming any ion beams, if $|V_{ex}| < 1$ volt $\sim \kappa T_e/e$. The Langmuir probe curves show that the change of the plasma potential is half of V_{ex} within this range of V_{ex}. If $|V_{ex}|$ is larger than 1 volt, an ion-beam is formed as shown in curve d. The ion flux from the driver plasma is limited by the ion thermal velocity, so that the driver plasma cannot supply enough ions for the target plasma potential to follow the applied potential difference.

The wave is excited by a sinusoidal voltage instead of a DC potential difference. Within the range $|V_{ex}| < 1$ volt, system excites the wave efficiently without forming any chopped ion beam.[16,17] In the low frequency range, $\omega << \omega_{pi}$ half of the applied voltage transferred into the potential of the wave, propagates in one direction from the grid, and the other half goes to another wave propagating in the opposite direction. In the high frequency range, $\omega \sim \omega_{pi}$, the coupling efficiency is decreased because of the finite transit time of the ions in the sheath around the grid.

A small plane Langmuir probe which is biased slightly

above the plasma potential is employed for the wave detection. The probe detects the electron saturation current which is proportional to the electron density. The spatial resolution of the detector is much better than the detector which collects the ion saturation current, since the probe electron sheath is thin.

A typical experimental dispersion curve for a small amplitude wave (perturbed to unperturbed density ratio $\tilde{n}/n_0 \sim 10^{-3}$) is shown in Fig.3. In the higher frequency range, the phase velocity is small. The solid curve shows the theoretical linear dispersion relation $\varepsilon(k,\omega) = 0$ for $T_e/T_i = 20$.

3. Experimental Results

When the wave amplitude is increased, and $\tilde{n}/n_0$ reaches several percent, the following nonlinear effects appear depending on the frequency, if the wave is nomochromatic. The received wave signals are shown in Fig.4 together with the excitation signal at three different frequencies.

(i) In the low frequency range ($\omega << \omega_{pi}$), the wave steepens and breaks into soliton peaks[11] (see upper two traces). As the frequency is increased, the number of peaks in one fundamental period is decreased.

(ii) Around the frequency where the dispersion curve starts deviating from a linear proportionality between ω and k (middle frequency range), the waveform is sinusoidal (see middle two traces). The measurements of spatial amplitude variation showed that the wave with large-amplitude continued propagating over a longer distance than a small amplitude

wave of the same frequency, being accompanied by the amplitude oscillation.[2] The depth of the amplitude oscillation, δn, is up to one fifth of $\tilde{n}$ in the present experiment. The depth damps away as the wave propagates after two or three oscillation periods as shown in Fig.5. Note that the amplitude oscillation is not due to the interference between the ion-acoustic wave and the chopped ion stream[18] because the wave excitation is different from the conventional grid exciattion. Even when we assume that the ions are accelerated by the amount corresponding to the excitation voltage, such an acceleration is insufficient to generate fast enough ions; i.e. the wave velocity is larger than $\sqrt{2eV_{ex}/M}$.

(iii) The primary interest of the present report is in the high frequency range where the phase velocity is significantly smaller than the ion-acoustic velocity. As seen on the bottom trace in Fig.4, a significant noise is observed to grow. Before describing the characters of the noise, let us examine the evolution of the ion distribution function in the presence of the large-amplitude wave.

A. Evolution of the Ion Distribution

The space and time resolved ion energy distribution is measured by an electrostatic energy analyzer combined with the sampling technique. Though it is favorable to measure the ion distribution in the high frequency range where the noise grows, the evolution of the ion distribution has been measured only in the middle frequency range, since the energy analyzer does not have a good enough spatial resolution to

measure the short scale length perturbations. Nevertheless the situation will not be different from that in the high frequency range. The interferometer output, plotted in Fig.6, shows that the wave amplitude oscillates in space initially, and then continues to propagate without damping. The ion energy analyzer curves (integrated energy distribution $\int_{\sqrt{\frac{2eV}{M}}}^{\infty} vf(v)dv$ vs. V) measured at each position (a, b, c and d) and at each phase of the wave (α, β, γ and δ), as specified in the sub-diagram, are presented at the bottom of the figure. In order to emphasize the tail of the distribution, only lower parts of the curves are shown.

At the stage where the wave amplitude decreases (position a), a group of ions is reflected by the wave potential and begins to form a bump in the distribution near the phase velocity (phase δ). At the position b where the wave amplitude grows, the bump is seen at phase β and γ; this fact means that the reflected ions eventually overtake the potential hill ahead of them. At the position where the wave amplitude is maximum (between b and c) no bump was observed (this is not shown in the diagram). This fact implies that the ions bounce back and the bump merges into the main body of the distribution. This cycle is observed also between the wave exciter and the first maximum point of the wave amplitude. After the second maximum, no clear bump is observed, but the distribution is slightly different from the exponential curve. The experimental results indicate that the main part of the trapped ions does not stay at the bottom of the wave potential but is near its top. Some part of the ions

may not bounce back but get over the potential hill. However, our analyzer system is unable to measure the amount of these ions.

In the case shown in Fig.6, the trapped-ion density is $5 \times 10^{-3}\ n_0$. The difference of the kinetic energy density of the trapped ions between the case when the ions are most accelerated and the case when they are most decelerated are estimated to be $2 \times 10^{-3}\ \kappa T_e n_0$. On the other hand, the difference of the wave energy density, $\omega(\partial\varepsilon/\partial\omega)|E|^2/8\pi$, between the case when the amplitude is maximum and the case when it is minimum is $3 \times 10^{-3}\ \kappa T_e n_0$. These two values are quite comparable.

B. Properties of the Sidebands

The frequency spectra of the signals received for several different carrier wave frequencies are displayed in Fig.7. In order to emphasize the sidebands, only lower amplitude parts of the spectra are shown. The wave excitation voltage is 1 volt from peak to peak and the distance from the grid to the receiver probe is 5 cm. Two types of sidebands are observed: the first is a group of distinct peaks separate from the carrier wave (type A), and the other consists of the structure around the foot of the carrier wave line (type B). If the carrier wave amplitude is increased starting from a very small value, growing type B sideband appears first, then the type A sidebands start growing when $\tilde{n}/n_0$ exceeds about 0.02. The frequency range, in which the type B sideband grows, starts from a lower frequency value respect to that where the

type A sideband is found.

Type A sidebands: As seen from Fig.7, the upper sidebands have a much smaller amplitude than the lower sidebands. Figure 8 shows the frequency spectra for various carrier amplitudes. As the amplitude is increased, the frequency separation between the sidebands and the carrier is increased. At larger amplitudes, the second lower sideband disappears first, then no sideband is observed except for the type B.

The equation (1a) accounts for the above properties of the lower sidebands. First of all, the ratio between the observed values of $(\omega/k) - (\omega_0/k_0)$ for the second and the first lower sidebands is in a range from 1.4 to 1.7. If we assume that the first and the second lower sidebands correspond to N = 0 and N = 1, respectively, the above ratio should be $\sqrt{3}$. By using the experimental dispersion curve and Eq.(1a), the bounce frequency is estimated. The estimated values of ω_B are plotted in Fig.9 as a function of $\tilde{n}/n_0$ (open circle). We have another two methods to obtain the value of ω_B; (1) from the period of the amplitude oscillations, and (2) from the relation,[19] $\omega_B = 2^{-1/4} k_0 \sqrt{e\phi_0/M}$. If we neglect the wave dispersion, this relation can be written as $\omega_B/\omega_0 = 2^{-1/4}\sqrt{\tilde{n}/n_0}$, which is shown in Fig.9 by the solid curve. Here we have used the relation $\tilde{n}/n_0 = e\phi_0/kT_e$. The values of ω_B obtained from the first method (dots) are significantly smaller than those obtained from the second method, but larger than the values from the sideband spectra. The discrepancy between the values found from the first and the second method may be due to the fact that the trapped-parti-

cles are not at the bottom of the wave potential trough. It should be mentioned that the condition (1a) and the dispersion relation (3) cannot be satisfied, if $\sqrt{2N+1}\ \omega_B$ is so large that $\sqrt{2N+1}\ \omega_B/k_0 > C_s - \omega_0/k_0$, where C_s is the ion-acoustic velocity. This fact explains why the sideband disappears when the carrier wave amplitude (and hence ω_B) is too large, as well as when ω_0 (and hence $C_s - \omega_0/k_0$) is too small.

Note that the frequency difference between the first lower sideband and the carrier is not the same as that between the first upper sideband and the carrier itself (Fig.7); therefore, the upper sideband is not the conjugate mode of the lower sideband but it is the one which satisfies (1b). However, the condition (1b) by itself does not account for the fact that no upper sideband grows when ω_0 is small.

The wavelength of the sideband is measured in the following way. Two probes are inserted in the plasma. The signals picked up from the probes are fed into a correlator through two independent narrow band filters (Q value $\simeq$ 100) tuned to the sideband frequency. The cross-correlation function is measured as a function of the position of one of the probes. The results of the measurements show that the sideband waves propagate along the direction of the carrier wave and that the wavelength of the lower sideband is shorter by a few percent than that of an externally excited ion-acoustic wave at the same frequency in the absence of the carrier. The amount of the shift in wavelength is comparable to the experimental errors mainly due to the finite filter width and to the slow drift of the voltage of the power supply feeding the machine.

But the shift is systematic.

The spatial growth of the first lower sideband is shown in Fig.10 (curve c). The band width of the receiver is narrower than the spectral line width of the sideband, therefore the total power in the sideband is larger than the one corresponding to the amplitude shown in the figure. The sideband grows initially and saturates in the most unstable case at a level comparable to that of the carrier wave. The initial spatial growth rate is observed to be approximately proportional to the square root of the carrier wave amplitude and can be expressed as $k_i = (0.1 \sim 0.2)\omega_B k_0/\omega_0$. This dependence of k_i on the wave amplitude excludes the possibility of other nonlinear processes such as nonlinear Landau damping.[20] The damping rate of the carrier wave is observed to be much greater when the sideband exists (curve a) than when it is absent, i.e. when the carrier wave amplitude is small (curve b) or when ω_0 is too small to excite sidebands (Fig.6).

In order to disturb the ordered motion of the trapped-ions, a wave, which is called perturbing wave, is excited in addition to the large-amplitude carrier wave. Since the wave is dispersive, it is expected that the two waves will propagate at different velocities, as a result the waveform deforms in a complicated way. Experiment shows that the type A sidebands are eliminated when the perturbing wave amplitude is comparable to that of the carrier. This fact may account for the saturation of the sideband. When the sidebands grow to an amplitude comparable to that of the carrier, the sidebands play the same role as the perturbing wave.

Type B sideband: The sideband of this type is observed in a wider range in ω_0 and in the carrier wave amplitude. The growth rate is approximately proportional to ω_B and almost the same as that of type A sidebands. This type of sideband is not destroyed by the perturbing wave. Low frequency noise, which corresponds to the difference frequency between the sideband and the carrier, is observed; however, the amplitude of the low frequency noise is very small compared to the sideband, so that it is attributed to the simple nonlinear mixing of the sideband and the carrier. These sidebands may reasonably be interpreted as those which satisfy the matching condition (2).

4. Discussion

We compare the experimental frequency spectra to the result predicted by Ref.7. Though Ref.7 has treated the electron plasma wave, its results can be applied to the ion-acoustic instability.

In order to know the explicit dispersion relation for the sideband, the particle distributions have to be given. We assume that the electrons follow the Boltzman relation and the carrier wave is stationary in the wave frame:

$$\phi(x) = \phi_0 \cos(k_0 x - \omega_0 t), \tag{4}$$

i.e. we neglect the amplitude oscillation. The ion distribution, $\Phi(x,v)$, when no sideband presents, can then be separated into the trapped-ion part, $\Phi_t(x,v)$, and the untrapped-

ion part, $\Phi_u(x,v)$:

$$\Phi = \begin{cases} \Phi_u & \text{for } |v-v_p| > \Delta(x) \\ \Phi_t & \text{for } |v-v_p| < \Delta(x) \end{cases}$$

where $v_p = \omega_0/k_0$ and

$$\Delta(x) = \{\frac{2e}{M}[\phi_0 - \phi(x)]\}^{\frac{1}{2}} . \qquad (5)$$

Since the carrier wave amplitude ($\tilde{n}/n_0 < 0.1$) is not very large, we choose the expression obtained by the linear theory for the distribution of the untrapped-ions:

$$\Phi_u(x,v) = f(v) - \frac{e}{M}\phi(x)\frac{1}{v-v_p}\frac{df(v)}{dv} , \qquad (6)$$

where $f(v)$ is the spatial average of the distribution. It has to be assumed that $f(v)$ is constant in the entire trapped region:

$$f(v) = f(v_p) \qquad \text{for } |v - v_p| < \Delta_M \qquad (7)$$

where

$$\Delta_M = (\frac{4e\phi_0}{M})^{\frac{1}{2}} .$$

Without this assumption, the second term on the RHS of Eq.(6) becomes greater than the first in the region $|v-v_p| < \Delta_M$,

and then the linear approximation cannot be accepted.

Using $\Phi_u(x,v)$ and $\phi(x)$ specified above, one can now uniquely determine $\Phi_t(x,v)$. To the order $\phi_0^{\frac{1}{2}}$, we have:

$$\Phi_t(x,v) = f(v_p) + a[\Delta^2(x) - (v-v_p)^2]^{\frac{1}{2}} \quad . \tag{8}$$

Note that (8) is similar to the trapped-particle distribution introduced by Bohm and Gross.[21] We define the excess trapped-ion density, Δn_t, by

$$\Delta n_t = \left\langle \int_{v_p-\Delta(x)}^{v_p+\Delta(x)} dv \Phi_t(x,v) \right\rangle - n_t \quad , \tag{9}$$

where

$$n_t = \left\langle \int_{v_p-\Delta(x)}^{v_p+\Delta(x)} dv f(v_p) \right\rangle = \frac{4}{\pi} \Delta_M f(v_p) \quad .$$

The angular bracket denotes the spatial average over a wavelength of the carrier, The quantity, a, can be written as

$$a = \frac{M}{\pi e \phi_0} \Delta n_t \quad . \tag{10}$$

Having specified the distribution $f(v)$ near $v = v_p$ as

$$f(v) - f(v_p) = \begin{cases} (v-v_p-\Delta_M)\alpha_+ & \text{for } v - v_p > \Delta_M \\ \\ (v-v_p-\Delta_M)\alpha_- & \text{for } v - v_p < \Delta_M \end{cases}$$

where

$$\alpha_{\pm} = - \frac{n_0}{\sqrt{2\pi}} \frac{v_p}{v_i} \exp[- \frac{(v_p \pm \Delta_M)^2}{v_i^2}] \quad ,$$

and

$$f(v_p) = \frac{n_0}{\sqrt{2\pi}} \frac{v_i}{v_p \Delta_M} \exp\ (- \frac{v_p^2}{2v_i^2}) \sinh(\frac{v_p \Delta_M}{v_i^2}) \quad ,$$

we can now derive the parameters appearing in the dispersion relation (34) in Ref.7. The final form of the dispersion relation is given as[22]

$$1 = \sum_{N=0}^{\infty} \frac{\omega_{pi}^2}{\Omega^2 - (2N+1)\omega_B^2} \frac{\omega_B}{\Omega} \frac{n_t}{n_0} [\frac{\Gamma_N^+}{\varepsilon(k,\omega)} + \frac{\Gamma_N^-}{\varepsilon(k-2k_0, \omega-2\omega_0)}] \quad , \tag{11}$$

where

$$\Gamma_N^{\pm} = \mu_N(\Omega) \frac{\Delta n_t}{n_t} + \nu_N(\Omega) \pm \gamma_N(\Omega) \quad , \tag{12}$$

and

$$\Omega = \omega - kv_p, \quad \text{and} \quad \omega_B^2 = k_0^2 \frac{e\phi_0}{M\sqrt{2}} \quad .$$

Choosing $k < k_0$ (i.e. $\Omega > 0$), we find the coefficients μ_N, ν_N and γ_N are positive. We also find ν_N to be much smaller than μ_N and γ_N, and hence we neglect ν_N hereafter.

If n_t/n_0 is very small, as in the case of the present experiment, the sideband waves are unstable when two of the denominators in (11) are nearly equal to zero.

We now discuss the sidebands which have discrete frequency spectra (type A). Depending on the value of $\Delta n_t/n_t$, we have three cases;

$$\text{(a)} \quad \Gamma_N^+ > 0 \quad \text{and} \quad \Gamma_N^- > 0, \quad \text{when} \quad \frac{\Delta n_t}{n_t} > \frac{\gamma_N}{\mu_N} \quad ,$$

$$\text{(b)} \quad \Gamma_N^+ > 0 \quad \text{and} \quad \Gamma_N^- < 0, \quad \text{when} \quad \frac{\gamma_N}{\mu_N} > \frac{\Delta n_t}{n_t} > -\frac{\gamma_N}{\mu_N} \qquad (13)$$

$$\text{(c)} \quad \Gamma_N^+ < 0 \quad \text{and} \quad \Gamma_N^- < 0, \quad \text{when} \quad \frac{\Delta n_t}{n_t} < -\frac{\gamma_N}{\mu_N} \quad .$$

It can easily be seen that a couple of waves, (ω,k) and $(\omega-2\omega_0, k-2k_0)$, are unstable at the frequencies which satisfy the following conditions:

$$\Omega \simeq \sqrt{2N+1}\,\omega_B \text{ and } \varepsilon(k-2k_0, \omega-2\omega_0) \simeq 0, \text{ for case (a)}, \qquad (14)$$

and

$$\Omega \simeq \sqrt{2N+1}\,\omega_B \text{ and } \varepsilon(k,\omega) \simeq 0, \text{ for case (c)}. \qquad (15)$$

In the case (b) no instability occurs. Note that no sideband grows[4] when $\Delta n_t = 0$ though $n_t \neq 0$. The condition (15) corresponds to (1a).

As pointed out in Section 3, the experimental results indicate that the type A lower sidebands are those which satisfy (1a). Therefore, the observed instability belongs to the case (c) in which $\Delta n_t < 0$ and not to the case (a). This conclusion may be consistent with the fact that the main part of the trapped-ions is not at the bottom of the potential well of the carrier. Recent theory by Bud'ka et al.[23] also

indicates that the distribution which was initially Maxwellian evolves to form holes in the trapped region.

The growth rate is calculated numerically from (11) by putting ω real and k complex for realistic values of the parameters. An example of the results is plotted in Fig.11 together with the experimentally observed spectrum which is obtained for parameters similar to those used in the calculation. The growth rate of the instability which satisfies (2) is not shown. Two sidebands corresponding to N = 0 and N = 1 grow and those corresponding to N > 1 do not grow both in the theory and the experiment.

The computed values of $k_i\omega_0/k_0\omega_B$ are around 0.1. The theoretical growth rate and frequency of the type A sideband, calculated by using a rather simplified ion distribution model, well account for the experimental results.

Equation (11) suggests that the wave which satisfies condition (2) is unstable in the case (c) in Eq.(13), therefore the presence of both type A and B sidebands under the same experimental conditions does not contradict Eq.(11). Differently from the type A, the wave has not necessarily to be dispersive to have the type B sideband. Since the condition (2) does not include ω_B, the type B instability can grow even when the perturbing wave disturbs the regular bounce motion of the trapped-ions.

5. Conclusion

Growth of the sideband waves is observed when a relatively large-amplitude monochromatic wave propagates in a

plasma having $T_e/T_i \gtrsim 20$. The conditions (1) and (2) well account for the frequency spectrum and for the range of the frequency and of the amplitude of the carrier wave in which the sideband waves grow. The sidebands extract the energy from the carrier and this in turn causes heavy damping of the carrier wave. Though the carrier wave in the present experiment is not perfectly the nonlinear stationary wave, the experimental results suggest that the B-G-K wave, which is accompanied with the trapped-ions, is unstable.

Acknowledgement

We are grateful to Dr. T. Sato of Kyoto University for valuable discussions.

References

1. I. B. Bernstein, J. M. Greene and M. D. Kruskal, Phys. Rev. 108, (1957)
2. C. B. Wharton, J. H. Malmberg and T. M. O'Neil, Phys. Fluids 11, (1968) 1761
3. W. L. Kruer, J. M. Dawson and R. N. Sudan, Phys. Rev. Lett. 23, (1969) 838
4. M. V. Goldman, Phys. Fluids 13, (1970) 1281
5. M. V. Goldman and H. L. Berk, Phys. Fluids 14, (1971) 801
6. W. M. Manheimer, Phys. Rev. A3, (1971) 1402
7. K. Mima and K. Nishikawa, J. Phys. Soc. Japan 30, (1971) 1722
8. W. L. Kruer and J. M. Dawson, Phys. Fluids 13, (1970) 2747
9. J. Denavit and W. L. Kruer, Phys. Fluids 14, (1971) 1782
10. R. J. Taylor, D. R. Baker and H. Ikezi, Phys. Rev. Lett. 24, (1970) 206
11. H. Ikezi, R. J. Taylor and D. R. Baker, Phys. Rev. Lett. 25, (1970) 11
12. L. M. Al'tsul and V. I. Karpman, Zh. Eksp. Teor. Fiz. 46, (1965) 515 [Sov. Phys. JETP 22, (1966) 361]
13. This does not mean that the distribution function must be oscillating with these frequencies when no sidebands are present.
14. B. D. Fried and R. W. Gould, Phys. Fluids 4, (1961) 139
15. H. Ikezi and R. J. Taylor, Phys. Fluids 13, (1970) 2348
16. I. Alexeff, W. D. Jones and K. Longren, Phys. Rev. Lett. 21, (1968) 878
17. H. Ikezi and R. J. Taylor, J. Appl. Phys. 41, (1970) 378

18. H. Ikezi, P. J. Barrett, R. B. White and A. Y. Wong, Phys. Fluids 14, (1971) 1997

19. Note that in the theory of Ref.12, the bounce frequency is given by $2^{-1/4}k_0\sqrt{e\phi_0/M}$ and not by the usual expression $k_0\sqrt{e\phi_0/M}$.

20. H. Ikezi and Y. Kiwamoto, Phys. Rev. Lett. 27, (1971) 718

21. D. Bohm and E. P. Gross, Phys. Rev. 75, (1949) 1851

22. Details of the derivation of the dispersion relation and of the related theoretical arguments will be reported in a separate paper by two of the present authors (K. M and K. N).

23. N. I. Bud'ka, V. I. Karpman and D. R. Shklyar, Zh. Eksp. Teor. Fiz. 61, (1971) 1463

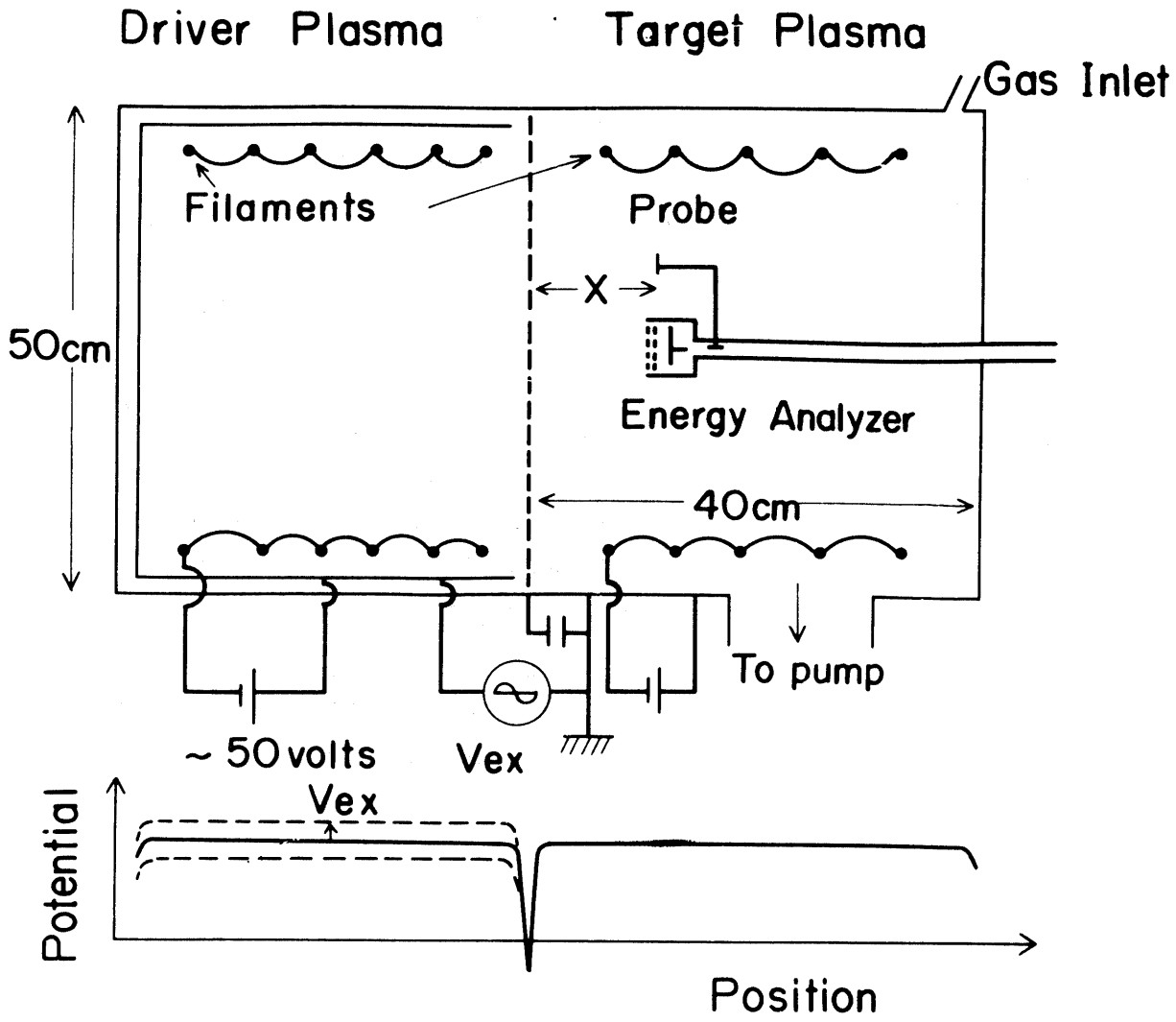

Fig.1 Layout of DP-machine. The potential profile is shown at the bottom.

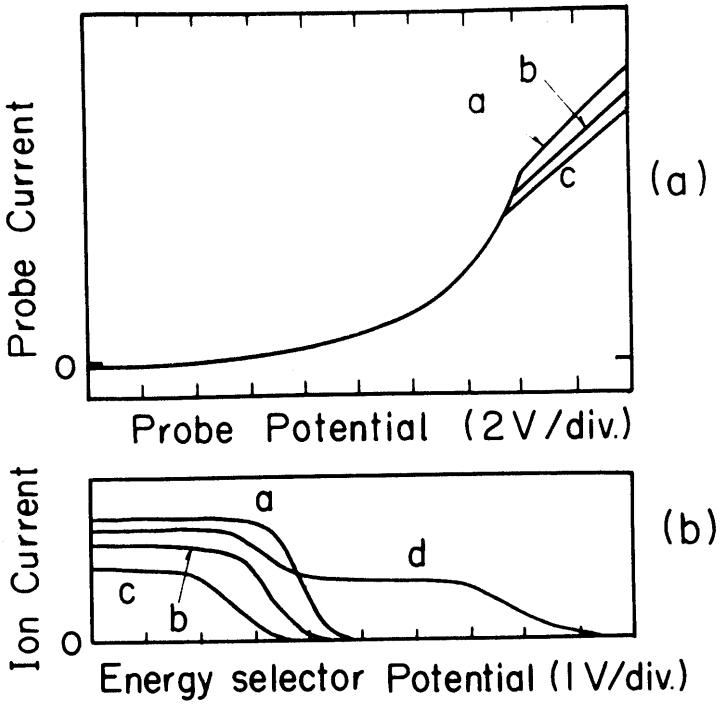

Fig.2 (a) Langmuir probe curves and (b) ion energy analyzer curves, when DC potential difference is applied between two plasmas. a; V_{ex} = 1 volt, b; V_{ex} = 0, c; V_{ex} = - 1 volt, and d; V_{ex} = 5 volts.

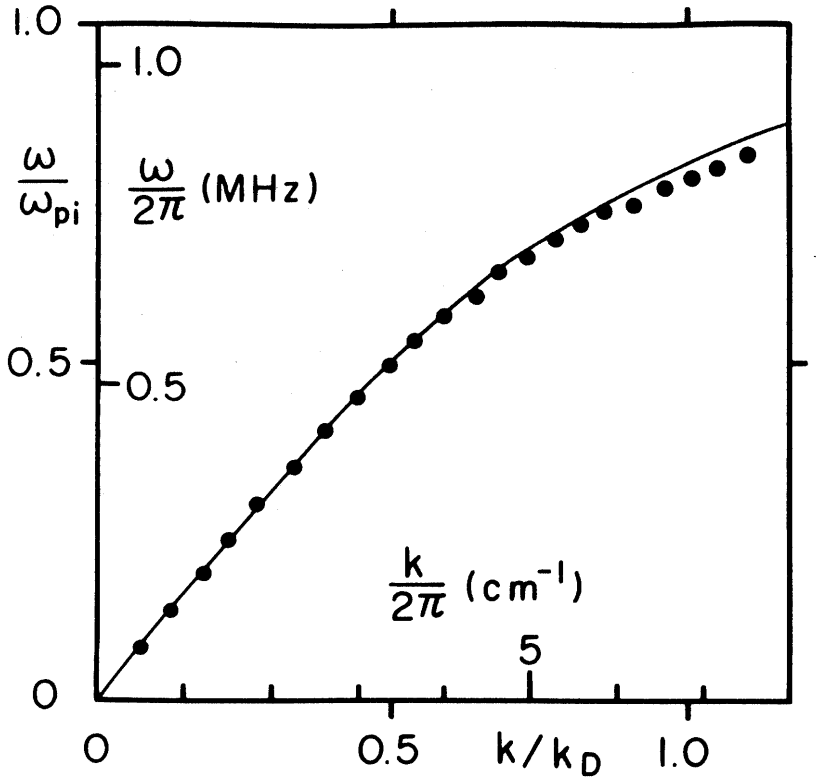

Fig.3 Dispersion relation of ion-acoustic waves. Dots are experimental points; curve shows Eq.(3) for $T_e/T_i = 20$.

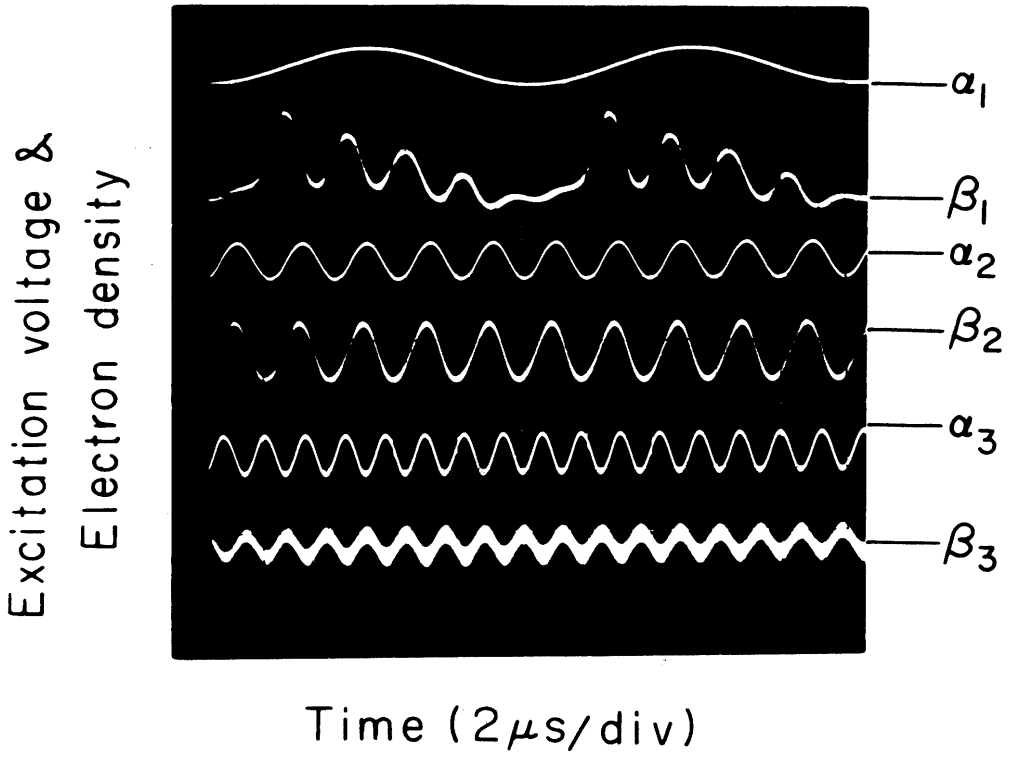

Fig.4 Excitation voltages V_{ex}, labeled by α (2 volts/div.) and perturbed electron density ñ, labeled by β (ñ/n = 0.1/div.), as a function of time. Excitation frequencies are 0.1 MHz for (α_1, β_1), 0.5 MHz for (α_2, β_2) and 0.8 MHz for (α_3, β_3). $\omega_{pi}/2\pi$ = 1.1 MHz. Distance from the wave excitation point, x, is 7 cm.

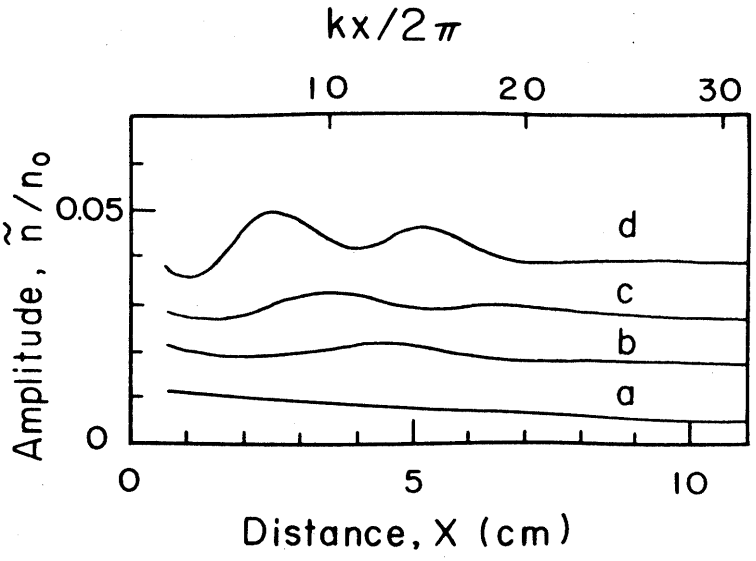

Fig.5 Wave amplitude, $\tilde{n}/n_0$, as a function of distance. $\omega/2\pi$ = 0.7 MHz. $\omega_{pi}/2\pi$ = 1.2 MHz. a; V_{ex} = 0.1 volt p-p, b; 0.3 volt p-p, c; 0.5 volt p-p, and d; 1 volt p-p.

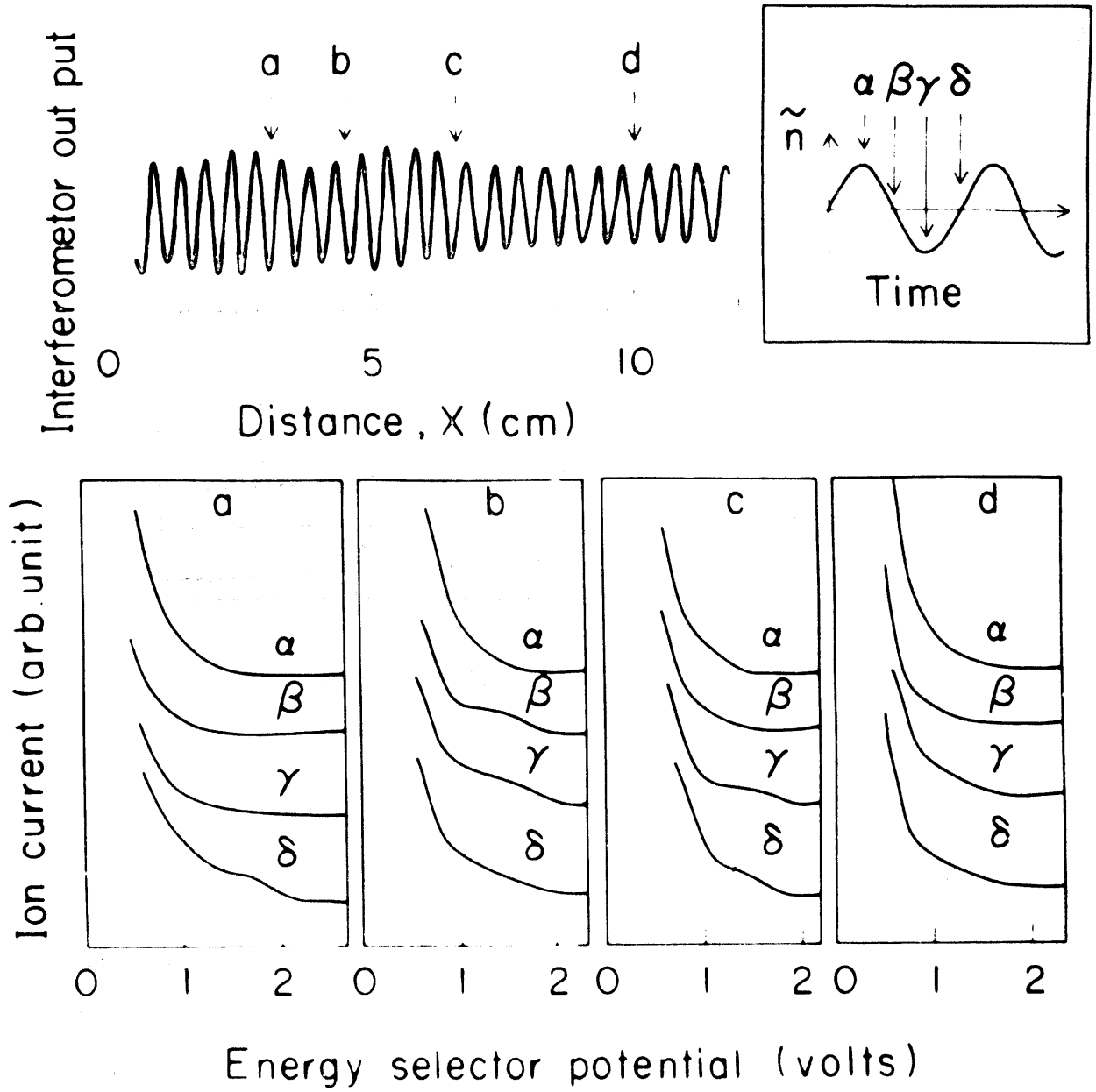

Fig.6 Ion energy analyzer curves at various positions (a, b, c and d), specified on the interferometer curve, and at various phase (α, β, γ and δ) of the wave specified in upper right sub-diagram. $\omega/2\pi$ = 0.5 MHz. $\omega_{pi}/2\pi$ = 1.2 MHz. V_{ex} = 1.2 volt p-p. The energy selector voltage ordinate, which is proportional to V^2, has the effect of making the bumb on the distribution seem broader than it is.

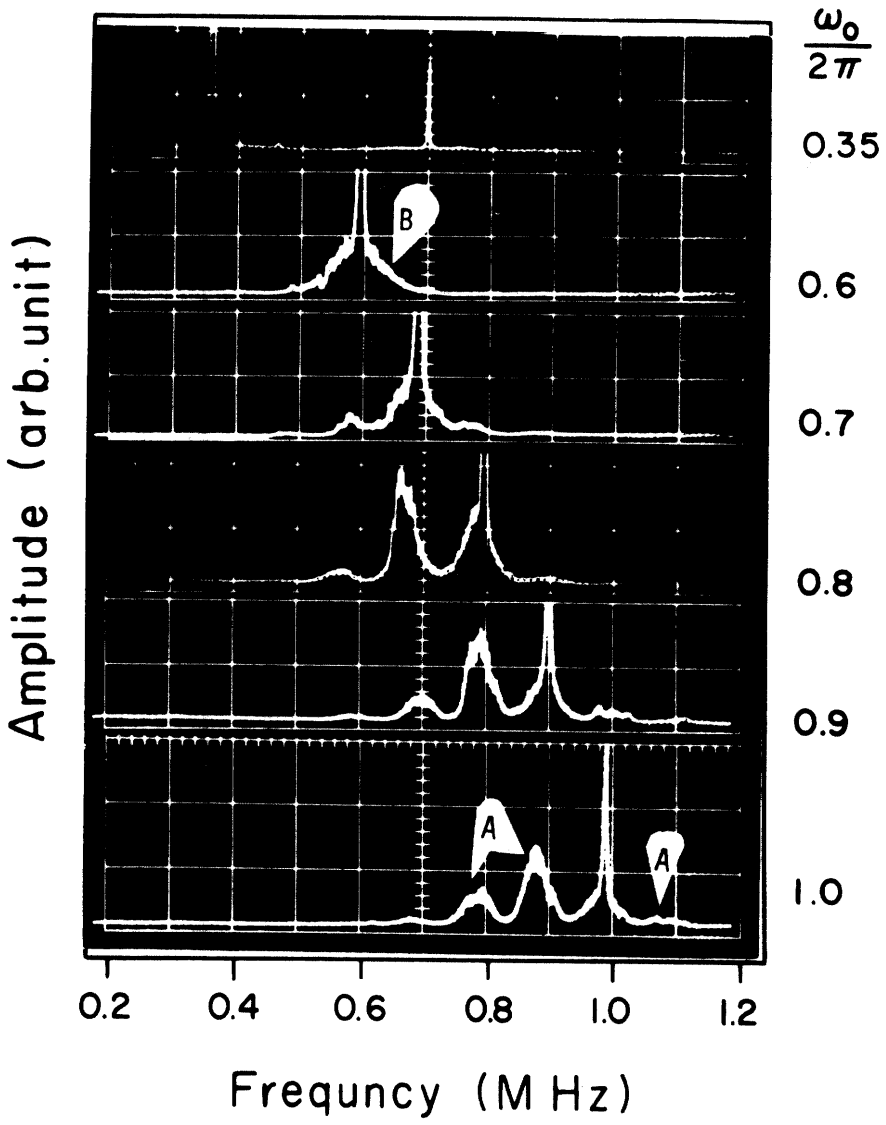

Fig.7 Frequency spectra of received wave signals at various ω_0. Only lower amplitude parts of the spectra are shown in order to emphasize the sidebands. $\omega_{pi}/2\pi$ = 1.3 MHz. x = 5 cm. V_{ex} = 1 volt p-p.

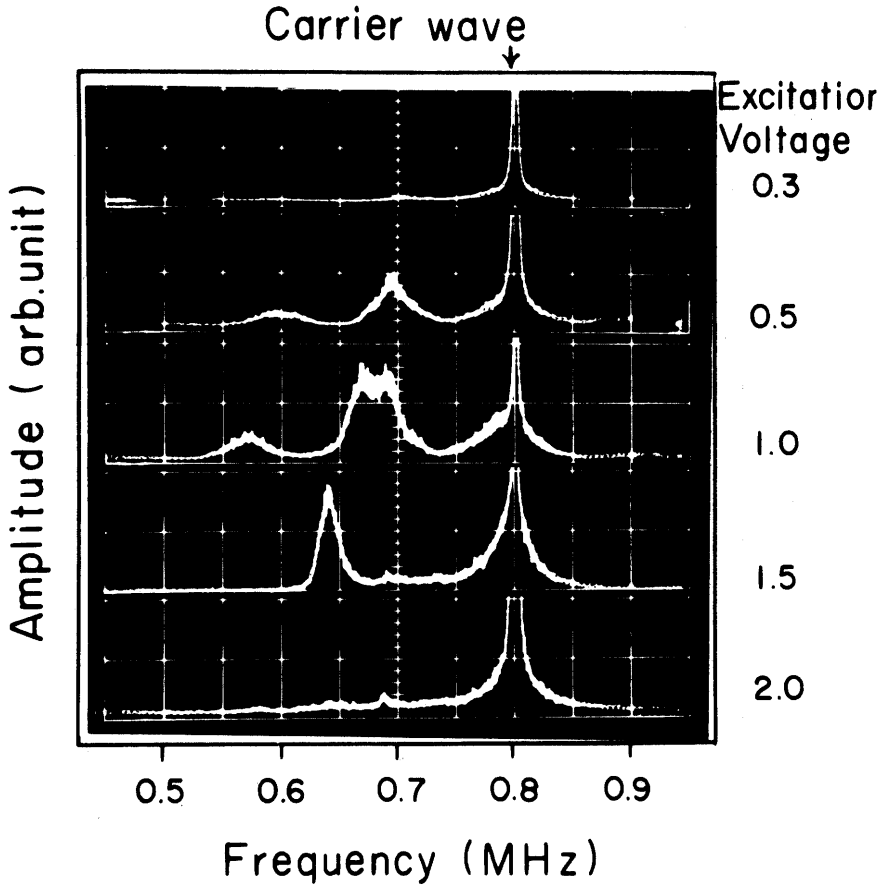

Fig.8 Frequency spectra of the sideband waves at various excitation voltage (peak to peak values are written). $\omega_{pi}/2\pi$ = 1.3 MHz. x = 5 cm. $\omega_0/2\pi$ = 0.8 MHz.

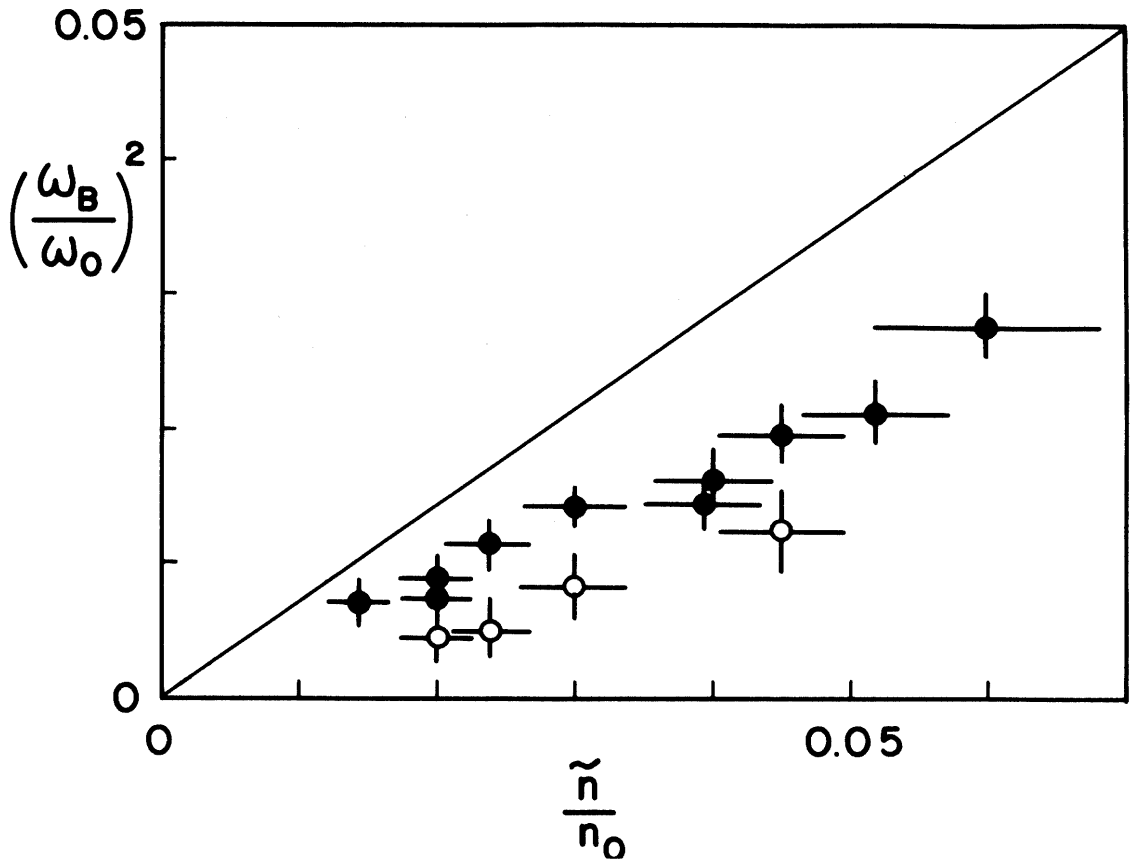

Fig.9 Bounce frequency as a function of wave amplitude. Solid line shows the relation $(\omega_B/\omega_0)^2 = \sqrt{2}\ \tilde{n}/n_0$. Dots are experimental points from the period of the amplitude oscillation. Open circles show ω_B obtained from the frequency of the sideband via Eq.(1a) and the experimental dispersion curve.

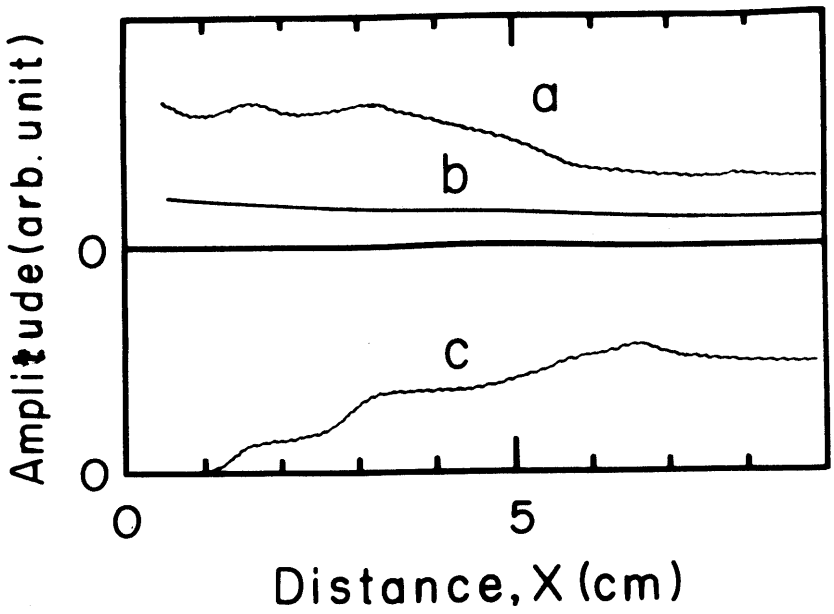

Fig.10 Amplitude of the carrier waves (a and b) and of the first lower sideband (c) as a function of distance. V_{ex} = 1 volt for curve a and c. V_{ex} = 0.3 volt for b. No sidebands grow in the case of curve c. Gain of the receiver is increased by 5 times for curve c. $\omega_0/2\pi$ = 0.8 MHz. ω_{pi} = 1.1 MHz.

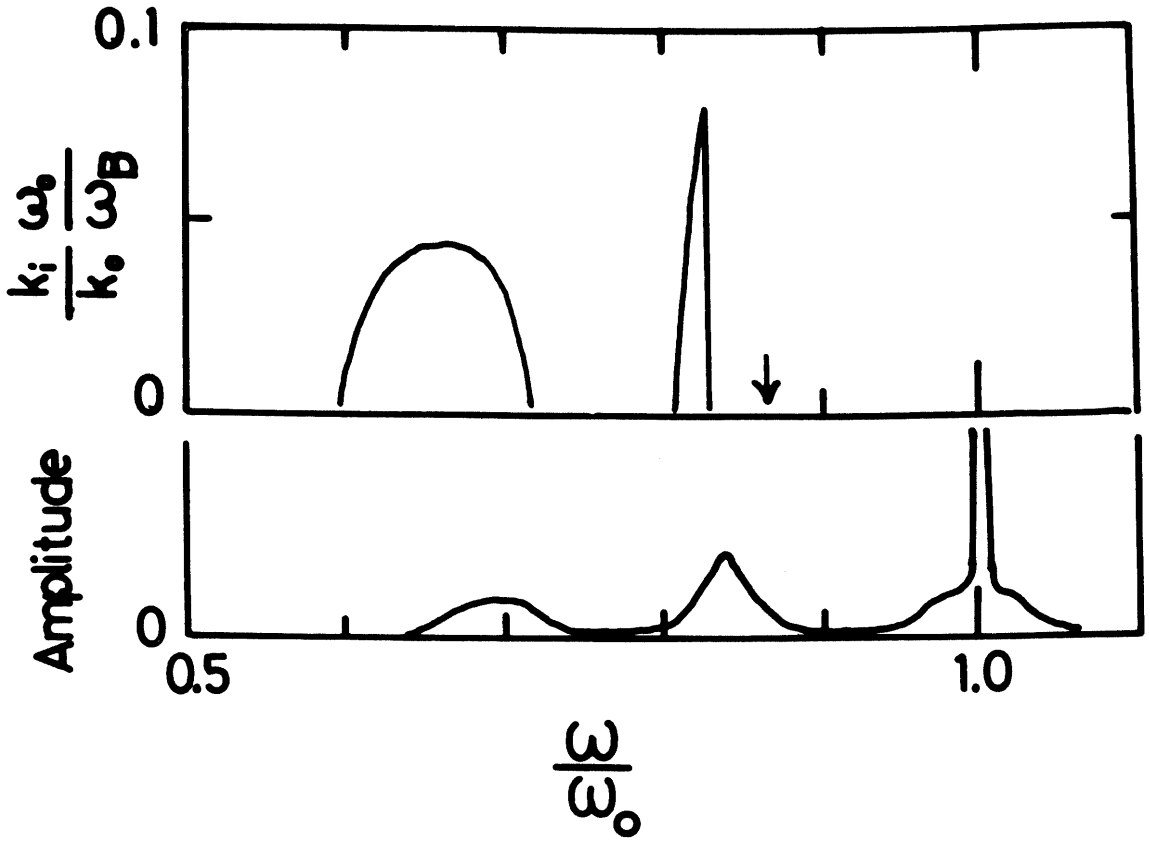

Fig.11 Upper diagram: Theoretical growth rate of the sideband as a function of frequency. Parameters are as follows; $\omega_{pi}/\omega_0 = 1.75$, $\omega_B/\omega_0 = 0.05$, $\Delta n_t/n_t = -0.36$, and $T_e/T_i = 20$. The arrow indicates the frequency predicted from (1a) for N = 0. Lower diagram: Experimental frequency spectrum. Parameters are as follows; $\omega_0/2\pi = 0.75$ MHz, $\omega_{pi}/2\pi = 1.2$ MHz, and $\omega_B/\omega_0 \simeq 0.1$.